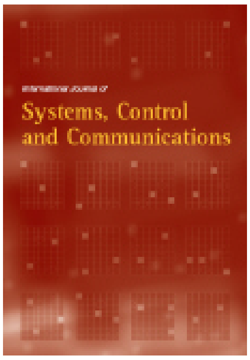

International Journal of Systems, Control and Communications

ISSN online: 1755-9359 - ISSN print: 1755-9340
https://www.inderscience.com/ijscc

Automation measures and power quality optimisation of power line carrier control based on electric spring and wavelet transform

Yegang Li

DOI: 10.1504/IJSCC.2026.10077009

Article History:

Received:	06 May 2025
Last revised:	13 June 2025
Accepted:	24 June 2025
Published online:	16 June 2026

Automation measures and power quality optimisation of power line carrier control based on electric spring and wavelet transform

Yegang Li

Suzhou Vocational and Technical College,
Suzhou Anhui, 234000, China
Email: 15955701608@163.com

Abstract: To promote sustainable energy production and support the development of renewable energy systems, this paper proposes a novel automatic detection and control optimisation framework based on electric springs and empirical wavelet transform. The principle of reactive power compensation realised by electric springs based on voltage vector relationships is analysed, and a topology optimisation scheme is proposed. The optimised electric spring can compensate for voltage disturbances within an operating range of 185.3 V–258.8 V, showing improvement compared to the original reactive power compensation control. Simulation results show that the instantaneous frequency of the voltage sag signal jumps at 0.399 s and 0.651 s, with actual errors of 0.25% and 0.15%, respectively. The small errors indicate that the start and end times of the voltage sag are accurately detected. This demonstrates that the power quality detection and control method proposed in this paper has high accuracy and significant advantages.

Keywords: power quality; renewable energy; reactive power compensation; electric spring; automate.

Reference to this paper should be made as follows: Li, Y. (2026) 'Automation measures and power quality optimisation of power line carrier control based on electric spring and wavelet transform', *Int. J. Systems, Control and Communications*, Vol. 17, No. 5, pp.1–18.

Biographical notes: Yegang Li obtained his BE in Automation from Anhui University of Science and Technology in 2005. He obtained his ME in Electrical Engineering from Anhui University of Science and Technology in 2012. Presently, he is working as an Associate Professor in the Department of Mechanical and Electrical Engineering, Suzhou Vocational and Technical College in Anhui. His areas of interest are Industrial automation technology and robotics technology.

1 Introduction

Smart grid reflects the progress of society and is an inevitable choice for the sustainable development of modern power grid. As for smart grid construction, different countries like the USA, Europe and Japan have different emphases, but their fundamental requirements for smart grid are consistent (Bebortta et al., 2024). The construction goals of smart grid in all countries include: compatible with distributed power generation and energy storage devices, and ensure the quality of power supply for users, which is the compatible and high-quality requirements of many functional characteristics of smart grid. To advance energy production and support the sound development of energy-saving, low-carbon industries and new energy sources, China has implemented policies aimed at actively promoting hydropower development, coordinating wind power development, and vigorously advancing distributed photovoltaic power generation. The emphasis in wind power development lies in consumption, necessitating the robust promotion of a novel power supply model that integrates incremental energy supply with smart grid technologies. Additionally, the development of low-voltage microgrid technology should be encouraged to facilitate local energy consumption (Chiam et al., 2023). In recent years, the power grid has frequently experienced issues of wind and solar power curtailment. The primary causes of this phenomenon can be attributed to the fluctuating and intermittent nature of distributed power supply output, which is influenced by natural factors. When integrated into the power grid, distributed power supply can significantly impact power quality, leading to problems such as voltage fluctuations, voltage flicker and harmonics (Shuo et al., 2014). These issues also pose challenges to the healthy development of the new energy industry.

As a classical signal analysis method, Fourier transform has many advantages such as orthogonal and complete, and has been frequently applied in power quality analysis. When using Fourier transform, the sampling theorem must be satisfied, and the signal to be analysed must be stable and periodically change with time (Errami et al., 2020). Otherwise, 'spectrum aliasing' and 'spectrum leakage' will occur in the FFT analysis results, which will affect the accuracy of the analysis. In addition, since the FFT transform is an integral over the entire time domain, the spectrum of any abrupt change in the signal will be spread over the entire frequency band, which cannot well reflect local information and is not fit in the analysis of abrupt and non-stationary signals in transient power quality (Savrun, 2021). The bimodal spectral line algorithm can be modified by using the two spectral lines after weighted average, which reduces the spectrum leakage in the power quality detection process of FFT method, and also improves the anti-noise interference ability (Gupta et al., 2022). Xiang et al. (2005) proposed a detection method combining FFT and neural network. The FFT algorithm in the paper is used for the pre-processing of interharmonics in order to improve the training speed of the neural network-based method (Xiang et al., 2005). At present, FFT algorithm is more used as a pre-processing tool for power quality analysis, so as to update the detection speed and accuracy of other algorithms.

For solving the power quality problem, according to electric spring reactive power compensation and empirical wavelet transform (EWT), this paper innovatively puts forward the power quality detection and control of renewable energy. First, working principle of the electric spring and the empirical wavelet change are presented. Under the background of analysing the voltage disturbance of power network, several types of reactive power compensation of ES are introduced, and the principle of reactive power compensation realised by ES in three modes is emphatically analysed according to the voltage vector relationship of ES in resistive, inductive and capacitive modes. Finally, to solve the problem that ES is easy to cause harmonics, the topology optimisation is proposed. The key innovations of this study are as follows:

1 A novel topology optimisation scheme for electric spring is proposed to expand its voltage compensation range from 205 V–240.4 V to 185.3 V–258.8 V.

2 An EWT-based voltage disturbance detection method is developed, achieving high accuracy in transient signal identification.

3 A combined harmonic and reactive power compensation control strategy is formulated to ensure critical load voltage stability under nonlinear conditions.

4 The simulation platform integrates MATLAB modelling and empirical data to validate the proposed methods, demonstrating small voltage detection errors (≤ 0.25%) and enhanced power quality control.

2 Electric spring and wavelet transform

2.1 Principle of electric spring

Figure 1 shows the simplified diagram of the connection of ES in an electrical framework. ES affects the operating voltage of non-critical loads in series by controlling their AC output voltage. Thus, ES and non-critical loads constitute intelligent loads and adjust the active and reactive power flowing to the load side, so that critical loads always work in rated conditions (Abou Hashem et al., 2018). Among them, non-critical loads are those that can undertake relatively large voltage fluctuations, like lighting systems, heating systems and cooling systems. Critical loads are those that have strict requirements on voltage, such as precision instrument manufacturing equipment and medical equipment (Solanke et al., 2022). Figure 1 shows the connection diagram of a single-phase full-bridge electric spring in the system. The AC side is an LC filter, and the filter capacitor and non-critical load are connected in series. The DC side is a capacitor. Compared with the DC side, the energy storage device is lower cost and easier to maintain. On the right side of the capacitor is an enable switch. When the switch is closed, the electric spring does not work, but when it is disconnected, the electric spring works normally.

The intelligent load composed of electric spring and non-critical load in series controls reactive power compensation on the one hand, and adjusts the power of non-critical load on the other hand. In Figure 1, the DC side of the electric bomb tube is a capacitor, which can only generate reactive power by itself. Therefore, when the DC side of the electric spring is a capacitor, the operation mode of the compensated reactive power can be divided into three forms. Capacitive reactive power compensation is carried out when the voltage value is lower than the reference value, and the electric spring voltage lags behind the non-critical load current (Wang et al., 2021). When the voltage value is higher than the reference value, the inductive reactive power compensation is carried out, and the electric spring voltage is ahead of the non-critical load current. When value of voltage is equal to the reference value, v_{es} is equal to 0. Non-critical loads show resistance characteristics, and the steady state operation of different loads is represented by solid and dotted lines of the vector, that is, the steady state operating point of the electric spring is affected by system parameters and actual voltage fluctuations (Mok et al., 2016). Whether it is capacitive or inductive, the amplitude of the output voltage of the electric cartridge has an effect on the amplitude of the non-critical load voltage and the phase of the critical load voltage.

Figure 1 Electrical spring system (see online version for colours)

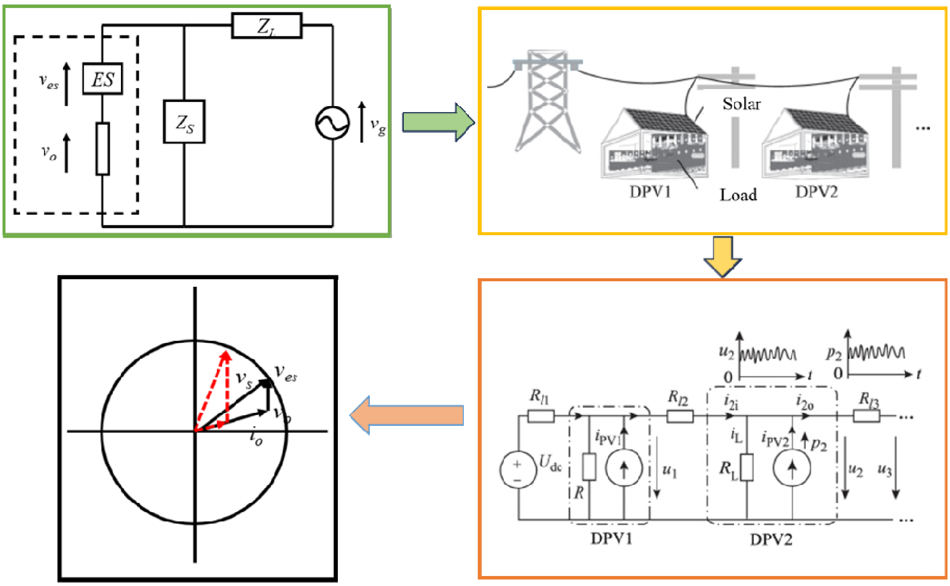

Select v_s as reference vector and get it from the vector diagram:

$$\begin{cases} P = V_s I \cos\varphi \\ Q = V_s I \sin\varphi \\ IX \sin\varphi + IR \cos\varphi = V_g \cos\delta - V_s \end{cases} \tag{1}$$

where V_s is the source voltage.

According to formula (1), when the transmission line presents resistance characteristics, there are:

$$\begin{cases} P = \dfrac{XV_g V_s \sin\delta + RV_s \left(V_g \cos\delta - V_s\right)}{X^2 + R^2} \\ Q = \dfrac{RV_g V_s \sin\delta + XV_s \left(V_g \cos\delta - V_s\right)}{X^2 + R^2} \end{cases} \tag{2}$$

where R and L represent the resistance and inductance of the transmission line, respectively; P is the active power; Q is the reactive power; δ is the phase angle between voltage and current.

When the transmission line is presented as perceptual, that is, $R = 0$, there are:

$$\begin{cases} P = \dfrac{V_g V_s \sin\delta}{X} \\ Q = \dfrac{V_s \left(V_g \cos\delta - V_s\right)}{X} \end{cases} \tag{3}$$

From equations (2) and (3), when the impedance of the transmission line presents resistance characteristics and sensitivity, the active and reactive power of the load have an impact on PCC voltage v_s (Lee et al., 2020). The critical load voltage can be adjusted by changing the amplitude and phase of the load voltage by controlling the active power and reactive power of the intelligent load.

$$i_{2i} - i_{2o} = i_L - i_{PV2} \tag{4}$$

$$u_2 = u_1 - i_{2i} R_{l2} \tag{5}$$

$$p_2 = i_{PV2} u_2 \tag{6}$$

From formula (4) to formula (6), the photovoltaic output current with fluctuation. Node voltage are combined, which is not easy to analyse the cause of voltage fluctuation.

2.2 Empirical wavelet transform

Assuming that the original signal is composed of N amplitude-FM components, EWT adaptively constructs wavelet filter banks to extract each mode component based on the Fourier spectrum of the signal (Wang et al., 2016). For selecting a suitable wavelet filter bank, the Fourier spectrum needs to be segmented adaptively. To satisfy the Shannon criterion, EWT normalises the Fourier spectrum to $[0, \pi]$.

The frequency range of the known signal is $[0, \pi]$, and the frequency domain is divided into N continuous bands without overlapping each other. Then, there are a total of $N + 1$ boundaries to be divided, where 0 and π are the spectrum's own boundaries, so the boundaries to be determined are $n - 1$.

$$\begin{gathered} \Lambda_n = [\omega_{n-1}, \omega_n], \quad n = 1, 2, \cdots, N \\ \bigcup_{n=1}^{N} \Lambda_n = [0, \pi] \end{gathered} \tag{7}$$

The method first detects several local maxima of the Fourier spectrum then arranges them in descending order. If the number of detected local maxima is greater than the band segmentation figure N, the first $n - 1$ maximum value is taken (Zhang and Zheng, 2020). If the number of local maxima is less than N, indicating that the component of the signal is less than expected, all detected local maxima are retained and N is reset. The boundary is then set to the midpoint of two consecutive local maxima, i.e.:

$$\omega_n = 0, \quad \omega_N = \pi, \quad \omega_n = (\Omega_n + \Omega_{n+1})/2, \quad (n = 1, 2, \cdots, N - 1) \tag{8}$$

First of all, the method is consistent with the 'local maximum midpoint' method to detect the local maximum of the spectrum, but the difference is that the boundary is set as the minimum value between two adjacent local maximum values, namely:

$$\omega_n = 0, \quad \omega_N = \pi, \quad \omega_n = \arg\min_{\omega} \Omega_n, \quad (n = 1, 2, \cdots, N - 1) \tag{9}$$

After determining each segment, the empirical wavelet is called bandpass filter on each segment (Liang et al., 2020). The empirical wavelet is constructed based on the construction idea of Littlewood-Paley and Meyer wavelet, and the empirical scale function and the empirical wavelet function are distinguished as equations (10) and (11):

$$\hat{\phi}_n(\omega)=\begin{cases}1 & |\omega|\le\omega_n-\tau_n\\ \cos\left[\frac{\pi}{2}\beta\left(\frac{1}{2\tau_n}(|\omega|-\omega_n+\tau_n)\right)\right] & \omega_n-\tau_n\le|\omega|\le\omega_n+\tau_n\\ 0 & \end{cases} \tag{10}$$

$$\hat{\psi}_n(\omega)=\begin{cases}1 & \omega_n+\tau_n\le|\omega|\le\omega_{n+1}-\tau_{n+1}\\ \cos\left[\frac{\pi}{2}\beta\left(\frac{1}{2\tau_n}(|\omega|-\omega_n+\tau_n)\right)\right] & \omega_{n+1}-\tau_{n+1}\le|\omega|\le\omega_{n+1}+\tau_{n+1}\\ \sin\left[\frac{\pi}{2}\beta\left(\frac{1}{2\tau_n}(|\omega|-\omega_n+\tau_n)\right)\right] & \omega_n-\tau_n\le|\omega|\le\omega_n+\tau_n\\ 0 & \end{cases} \tag{11}$$

The definition of the empirical wavelet seriously change is very comparable to that of the classical wavelet transform. The empirical wavelet radically change can be developed by way of the usage of the classical wavelet seriously change method. Its approximation coefficient and element coefficient are decided as the internal product of the authentic sign and the empirical scale feature and the empirical wavelet characteristic respectively:

$$W_f^{\varepsilon}(0,t)=\langle f,\phi_1\rangle=\int f(\tau)\overline{\phi_1(\tau-t)}d\tau=\left(\hat{f}(\omega)\overline{\hat{\phi}_1(\omega)}\right)^{\vee} \tag{12}$$

$$W_f^{\varepsilon}(n,t)=\langle f,\psi_n\rangle=\int f(\tau)\overline{\psi_n(\tau-t)}d\tau=\left(\hat{f}(\omega)\overline{\hat{\psi}_n(\omega)}\right)^{V} \tag{13}$$

The signal of the example is formed by the superposition of three component signals, as shown in equations (14) and (15) and Figure 2. Where component 1 is a DC component, and other components are AC components.

$$f_1(t)=4t+1,\quad f_2(t)=\sin(10\pi t),\quad f_3(t)=0.5\sin(50\pi t) \tag{14}$$

$$f(t)=f_1(t)+f_2(t)+f_3(t) \tag{15}$$

Spectrum segmentation Figure 2 shows that the original signal spectrum is divided into three parts, and the spectral peaks of each AC component (component 2 and component 3) are within their respective segmentation ranges. EWT completes spectrum adaptive segmentation according to frequency domain characteristics. Compared with Figure 2, the original signal is decomposed into three mode components by EWT. For the AC modes (modes 2 and 3), the standard sinusoidal waveform is presented regardless of the endpoint part. The waveform of each modal component is very similar to that of the original component, and each modal component is successfully separated without modal aliasing (Anu et al., 2020). The reconstructed signal is also very similar to the original Xin5 signal, indicating that EWT has a good mode decomposition ability for multi-frequency steady-state signals (including DC components).

Figure 2 Test signal and decomposition results

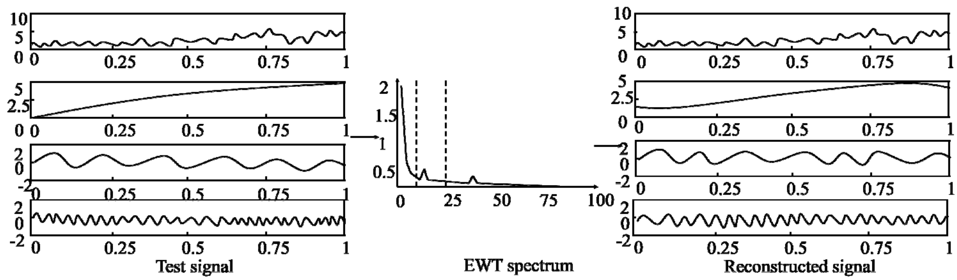

3 Reactive power compensation of power system based on electric spring

3.1 Reactive power compensation analysis of ES

Ensuring the voltage consistency at both ends of the critical load, ES needs the reactive power and inject dynamic reactive power compensation into the grid through the function of the inverter. The control of reactive power by ES can be divided into phase control and amplitude control. When ES realises reactive power compensation, the reactive power property of its inverter voltage source should be opposite to that of the reactive power disturbance source in generation side, so as to achieve the due compensation effect (Chen et al., 2022). When inductive disturbance occurs on the generation side, the reactive compensation voltage of ES is capacitive to offset the disturbance caused by inductive reactive power to the grid. At this time, ES works in capacitive mode, and its compensating voltage phase lags behind the current by 90°. On the contrary, when there is capacitive disturbance on the generating side, ES works in inductive mode, and its compensation voltage phase is 90° ahead of the current. Therefore, the phase properties of ES reactive compensation voltage depend on the type of reactive disturbance on the generating side.

$$\begin{aligned} V_g &= V_s + V_z \\ V_s &= V_{es} + V_o \end{aligned} \tag{16}$$

Reactive power compensation analysis in resistive mode

When ES works in resistive mode, the AC power supply voltage of the power grid is stable, and no reactive power disturbance of any nature is emitted, and the demand side does not need ES for voltage regulation. Therefore, its output voltage V is zero, and there is no non-functional quantity exchange between ES and the system, so the phase control of reactive power compensation voltage is meaningless (Fu et al., 2021). Relative to the entire grid, the effect of line impedance is negligible, so:

$$V_g = V_s = V_o \tag{17}$$

In the energy grid, the critical load is in parallel with the non-critical load, so the critical load voltage remains constant and consistent with power grid voltage.

Figure 3 ES simulation model of reactive power compensation control (see online version for colours)

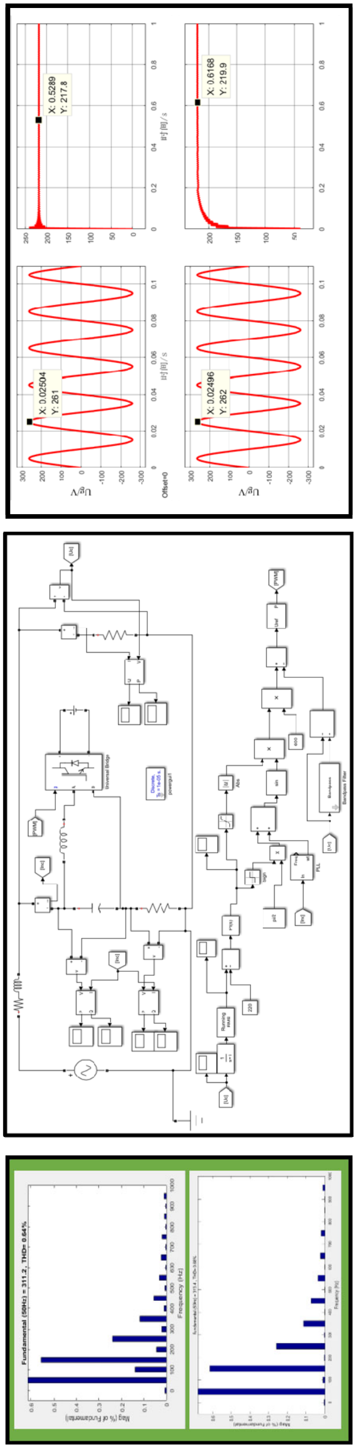

Reactive power compensation analysis in inductive mode

When the AC energy grant of the electricity grid injects capacitive reactive strength disturbance into the energy grid, ES will work in inductance mode to elevate out inductive reactive energy compensation to the system, so as to offset effect of the capacitive reactive strength disturbance. Under such conditions, the grid voltage is often higher than the normal value to be maintained. Reactive power compensation devices are required to absorb reactive power from the system to offset reactive power disturbance, so as to reduce voltage at compensation point and maintain the voltage stability of the grid (Yang et al., 2020). Meanwhile, output voltage segment of ES is orthogonal to the non-critical load voltage segment and 90° ahead, and its characteristic is equal to a pure inductor. The output voltage amplitude of ES can be managed via constantly altering its inductive reactance value, so as to dynamically take in the reactive electricity of the system.

Reactive power compensation analysis in capacitive mode

The reactive energy compensation precept of ES running in capacitive mode is precisely contrary to that of inductive mode. In this mode, the AC strength grant injects inductive reactive strength disturbance into the grid, and the output voltage section of ES is orthogonal to the non-critical load voltage phase, with a lag of 90°. ES wishes to compensate the inductive reactive strength of the gadget to offset the have an effect on of the inductive reactive energy disturbance. Under such conditions, the grid voltage is frequently decrease than the regular cost to be maintained, and reactive energy compensation units are required to launch reactive strength from the gadget to offset reactive electricity disturbance (Zou et al., 2019). At this time, ES can be equal to a capacitor that dynamically and continually modifications its capacitance and injects reactive electricity into the machine to expand the voltage at the compensation factor and hold the voltage steadiness of the grid in accordance to the wants of the voltage at the compensation point.

Because the frequency of harmonic components in the usual system is not fixed, it is impossible to filter out all harmonics. Not only that, because the shunt filter is of low impedance to harmonics, the harmonic source will produce a larger harmonic current, and the filters resonant at different frequencies will interfere with each other, for example, the seventh harmonic filter may amplify the fifth harmonic. LC low-pass filter has a good effect on filtering out the interference of low harmonic to a certain extent. However, it cannot suppress high-frequency harmonics, so the filtering effect of LC low-pass filter is not stable.

Nowadays, LCL filter has been used and studied more, because PWM control strategy is usually adopted in grid-connected inverters. But there are rich switching harmonics in the output PWM voltage, in order to suppress the switching harmonics in the grid-connected current. Therefore, LCL filter is generally used as output of grid-connected inverter, and its structure is mainly composed of two inductors and a capacitor. The circuit relationship can be obtained:

$$\begin{aligned} & i_1 = i_2 + i_3 \\ & G_{LCL}(s) = \frac{I_2(s)}{U_{in}(s)} \end{aligned} \tag{18}$$

Ignoring the influence of the power line impedance and inductance resistance, equation (18) can be expressed as:

$$\begin{aligned} G_{LCL}(s) &= \frac{I_2(s)}{U_{in}(s)} \\ &= \frac{R_d C s + 1}{L_1 L_2 C s^3 + (L_1 R_{nc} + L_1 R_d + L_2 R_d) C s^2 + (L_1 + L_2 + R_{nc} R_d C) s + R_{nc}} \end{aligned} \tag{19}$$

To illustrate, let:

$$\begin{aligned} L &= L_1 + L_2 \\ L_1 &= pL \end{aligned} \tag{20}$$

This can be simplified as:

$$G_{LCL}(s) = \frac{R_d C s + 1}{p(1-p) L^2 C s^3 + (pLR_{nc} + LR_d) C s^2 + (L + R_{nc} R_d C) s + R_{nc}} \tag{21}$$

Compared with LC low-pass filter, the filter capacitor in LCL filter provides bypass path for high frequency harmonic current, and has the advantages of small size, low cost and low power consumption. However, the frequency response of the LCL filter has a resonance spike, and the phase will have a negative 180° jump at the resonance frequency. If the resonance spike is not effectively damped, the output current of the grid-connected inverter may oscillate and even lead to system instability (Yu and Zhang, 2025). According to the different realisation methods, the damping methods to solve the resonant peak can be divided into passive damping method and active damping method. Active damping method is easy to implement. However, this method will only change the frequency characteristics near the resonant frequency, which has little impact on low and high frequency bands, and the damping resistance loss is large, which will lead to lower efficiency, so this method is not practical. The passive damping method is to filter the capacitor branch resistance in series, select a suitable damping resistance to effectively damp the resonant peak, and the damping resistance loss is small, and has good stability. The value of damping resistance has obvious influence on the harmonic suppression effect of LCL filter. When damping resistance is close to zero, the resonant amplitude is large and the filter performance is poor. When the value of damping resistance is too large, all the frequency bands decay, which increases the damping loss to a certain extent.

3.2 Optimisation simulation

When U_g RMS value is 205 V (amplitude 290 V) in Figure 3, the harmonic content of critical load voltage after adopting two optimisation schemes is 0.64% and 0.8%, respectively. The experimental results show that both schemes can achieve the effect of suppressing the harmonics of the critical load voltage, but the operation of scheme 2 is simple, so this section focuses on the simulation analysis of scheme 2.

After the reactive power compensation control of scheme 2 is adopted, the simulation results show that ES can compensate the disturbance voltage (effective voltage) in the working range of 185.3 V–258.8 V. Compared with the original control (205 V–240.4 V), ES not only improves the working range of ES but also improves the voltage distortion rate of key loads. The specific waveform after simulation is as follows.

When U_g RMS value is 184.5 V (amplitude 261 V), the waveform of RMS value of U-shaped and critical load voltage is shown in Figure 3. When U_g is 184.5 V, ES cannot restore the critical load voltage to the ideal value of 220 V. When U_g is 185.3 V, ES can restore the critical negative voltage to the ideal value of 220 V, so 185.3 V is the lower limit of disturbance voltage that ES can compensate.

In summary, ES with optimised reactive power compensation control can compensate the disturbance voltage in the operating range of 185.3 V–258.8 V, and the voltage compensation capability of ES is improved compared with the original reactive power compensation control. In the comparative analysis, the harmonic content of the key load voltage is reduced from 14%~16% to 0.68%~2.21%. The optimised reactive power compensation control can improve the ES voltage compensation ability and reduce the harmonic content of the key load voltage.

4 Power quality control of electric spring under nonlinear load

4.1 Current detection method

When the electric spring fails, the switch *S* closes. Because the existence of harmonic current source and equivalent impedance, the current flowing through the key load and power side will contain harmonic and reactive components. The bus voltage will also contain harmonic, resulting in the decline of power quality (Wang et al., 2020a; Yang et al., 2016).

$$\begin{cases} i_s = i_{s1p} + i_{s1q} + i_{sh} \\ i_c = i_{c1p} + i_{c1q} + i_{ch} \\ i_{es} = i_{es1p} + i_{es1q} + i_{esh} \end{cases} \tag{22}$$

According to KCL theorem:

$$i_s = i_c - i_{es} \tag{23}$$

The expression of reactive power component and harmonic component can be obtained as follows:

$$\begin{cases} i_{sh} = i_{ch} - i_{esh} \\ i_{s1q} = i_{c1q} - i_{es1q} \end{cases} \tag{24}$$

After the electric spring is compensated for harmonic and reactive power, the current will not contain harmonic and reactive power components, that is:

$$\begin{cases} i_{sh} = i_{ch} - i_{esh} = 0 \\ i_{s1q} = i_{c1q} - i_{es1q} = 0 \end{cases} \tag{25}$$

Solving formula (25) yields:

$$\begin{cases} i_{esh} = i_{ch} \\ i_{es1q} = i_{c1q} \end{cases} \tag{26}$$

If the equation of formula (26) is true, then the current contains only the fundamental active component, and the harmonic and reactive components are compensated, then the bus voltage is:

$$v_s = v_g - i_{s1p} Z_S = v_g - \left(i_{c1p} - i_{es1p}\right) Z_S \tag{27}$$

From formula (27), while harmonics and reactive power compensation are realised, the bus voltage can be adjusted by controlling the active component of fundamental wave that flows through the electric spring current to achieve voltage regulation (Nagalakshmi et al., 2022). The voltage can be stabilised by a PI controller, and the transfer function of the controller is:

$$\begin{aligned} & i_{es1p}(t) = K_P e(t) + \frac{K_P}{T_i} \int_0^t e(t) dt \\ & e(t) = V_{S\_ref} + V_S \end{aligned} \tag{28}$$

The current flowing through the electric spring can be calculated, and then through the KVL theorem, the compensation voltage of the electric spring can be calculated as:

$$v_{es} = v_s + i_{es} Z_{NC} \tag{29}$$

By detecting the load harmonic current, the harmonic present day command fee of the electric powered spring is calculated. The fundamental reactive cutting-edge of the load is measured and the command price of the fundamental reactive modern-day of the electric powered spring is calculated. The error between the bus voltage and the rated reference voltage is detected, and the training price of the indispensable lively modern of the electric powered spring is got via PI adjustment (Wang et al., 2020b). The sum of indispensable modern-day and harmonic contemporary is the compensation cutting-edge of the electric powered spring, and the command cost of the electric powered spring voltage is acquired via system [formula (29)]. Through dynamic detection and compensation, the electric spring ensures that the current and bus voltage do not contain harmonic components, while stabilising the bus voltage to the rated value. The harmonic compensation of electric spring needs to detect the harmonic current on the load side. In the harmonic current detection of three-phase circuit based on the instantaneous reactive power theory, the phase signal of the fundamental active and reactive components of the load current is generated after the grid voltage is passed through the phase-locked loop (Tapia-Tinoco et al., 2020). The load current is transformed by coordinate through the phase signal, so that the fundamental wave and harmonic frequency are all reduced once, and the fundamental wave component becomes the direct flow. The harmonic component is the AC amount that the frequency is reduced once, and then the AC amount is filtered through the low-pass filter which is the harmonic signal. The direct flow is obtained, which is the fundamental signal. Then, the fundamental current is obtained by inverting the phase signal, and the harmonic current is obtained by comparing with the original current.

4.2 Electric energy control strategy of electric spring under nonlinear load

To calculate reactive power and harmonic compensation components of the electric spring, it is necessary to solve the sum of the harmonic and reactive power components of the current at the key load side. From formula (30):

$$i_{ch} + i_{c1q} = i_c - i_{c1p} \tag{30}$$

This paper adopts the detection method based on the instantaneous reactive power theory. The specific steps are as below:

- make supply voltage:

$$v_g(t) = \sqrt{2}V_g \cos \omega t \tag{31}$$

- the key load current is:

$$i_c(t) = \sum_{n=1}^{\infty} \sqrt{2}I_{cn} \cos\left(n\omega t + \varphi_n\right). \tag{32}$$

Under nonlinear load, due to the existence of nonlinear load Z_c, both power supply side current and the bus voltage contain harmonics. Current also contains reactive power component. First, the power supply side voltage is phase tracked through the PLL, and the current and cos *wt* are multiplied. Then, the effective value of the active component of the fundamental wave can be obtained by filtering the AC component through the second-order low-pass filter and enlarging it by two times. Finally, the instantaneous value of the active component of the fundamental wave can be obtained by multiplying the effective value with the cos *wt* obtained by the PLL.

In order to maintain the stability of the bus voltage, the bus voltage regulation ring is added into control strategy. By detecting the effective value of the bus voltage and comparing it with the rated reference value 220 V, the effective value of the fundamental active power component of the electric spring current is obtained by PI controller, and the extracted fundamental active power effective value is offset. Finally, the fundamental active component of the current at the power supply side is obtained, which is the command value. The electric spring current command value can be obtained by subtracting the i_s command value from i_c, and the electric spring voltage command value can be obtained by formula (29). The electric spring can realise harmonic and reactive power compensation and voltage regulation function under nonlinear load, thereby improving power quality and grid operation efficiency.

4.3 Power quality disturbance detection simulation

Firstly, several common disturbances in the power system are modelled by mathematical means, and six disturbance signals of voltage sag, voltage rise, voltage interruption, harmonics, transient pulse and transient oscillation as shown in the following table are established. The corresponding disturbance signal waveform is generated in MATLAB simulation software, and the improved wavelet transform method is applied to analyse them.

According to the mathematical model of six single disturbances, simulation waveform is generated by MATLAB simulation software with sampling frequency of

5 kHz and signal base frequency of 50 Hz. The parameters corresponding to specific disturbances are set as follows:

1. Voltage dip signal: The temporary drop value is set to 0.8 times of the normal value, the temporary drop value is 62.22 V, the start and stop time $t1$ and $t2$ are set to 0.4 s and 0.65 s respectively, and the simulation time is set to 1 s.
2. Voltage temporary rise signal: The temporary rise value is set to 1.4 times of the normal value, the temporary rise value is 435.51, the start and stop time tl and $t2$ are set to 0.4 s and 0.65 s respectively, and the simulation time is set to 1 s.
3. Voltage interruption signal: Amplitude drop is set to 0, start and end time $t1$ and $t2$ are set to 0.4 s and 0.65 s respectively, and simulation time is set to 1 s.
4. Interharmonic signal: The fundamental amplitude is set to $220\sqrt{2}$, including five harmonics, the amplitude is $100\sqrt{2}$, the start and end time $t1$ and $t2$ are set to 0.35 s and 0.65 s respectively, and the simulation time is set to 1 s.
5. The fundamental amplitude is set to 1: The frequency is set to 50 Hz; the start and end time tl and $t2$ of transient oscillation are set to 0.082 s and 0.096 s, respectively; the oscillation al is set to 0.6; $f1$ is set to 500 Hz; the simulation time is set to 0.2 s.
6. The fundamental amplitude is set to $200\sqrt{2}$: The frequency is set to 5 Hz; the start and end time $t1$ and $t2$ of the transient pulse are set to 0.5 s and 0.505 s, respectively; the pulse amplitude al is set to 200.

For the detection and analysis of a single power quality disturbance, steps are as follows:

1. Generate various types of single power quality disturbance signals.
2. For the voltage dip, voltage rise and voltage interrupt signals of single signal components, EMD decomposition and HT analysis of the signals are performed by using EWT way. The improved HHT approach is applied to decompose inter-harmonic signal, transient oscillation signal and transient pulse signal with intermittent and instantaneous characteristics and analyse the EMD spectrum.
3. According to the decomposition results, the instantaneous characteristics of the signal are extracted.

The HHT analysis of the six single disturbance signals in the previous section is as follows.

4.3.1 Voltage dip signal wavelet analysis

In Figure 4 and Table 1 that the IMF1 component of the voltage sag signal retains the characteristics of the signal sag well after EMD decomposition. The wavelet analysis displays that the instantaneous rate of the voltage dip signal changes at 0.399 s and 0.651 s, and the actual error is 0.25% and 0.15%, respectively. The error is small, and the starting and ending time of the voltage dip is accurately detected. Meanwhile, through analysis of the instantaneous amplitude data matrix, detected voltage amplitude drops to 62.55 V. The error with the theoretical amplitude is 0.53%.

Figure 4 Transient frequency and amplitude of the signal (see online version for colours)

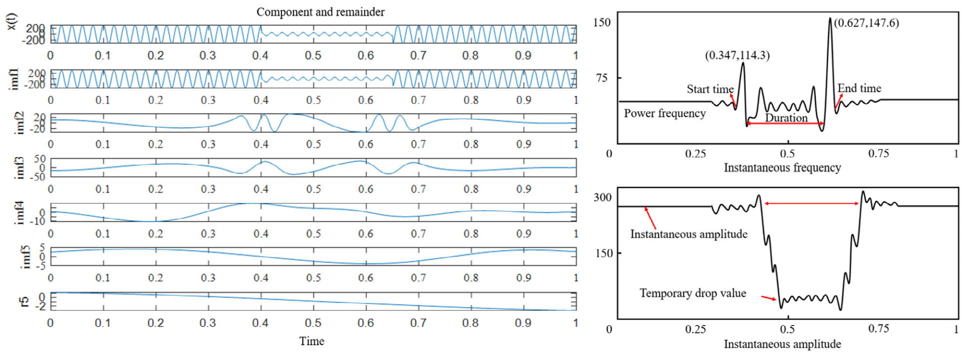

Table 1 Test results of voltage sag signal

Detection parameter	*Theoretical value*	*Actual value*	*Deviation*
Initial time	0.41	0.399	0.25%
End time	0.652	0.651	0.15%
Amplitude	62.23	62.55	0.53

Figure 5 Transient frequency and amplitude of transient signal (see online version for colours)

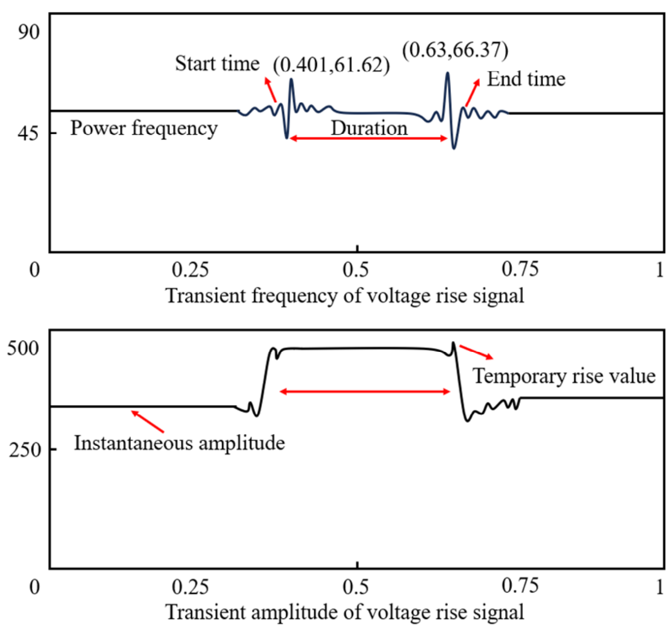

4.3.2 EWT analysis of voltage temporary rise signal

It can be inferred Figure 5 that IMF1 content of voltage ramp signal preserves the characteristics of the signal ramp well after EMD decomposition. The wavelet analysis looks like that the instantaneous frequency of the voltage dip signal changes at 0.401 s and 0.65, and the actual error is 0.25% and 0, respectively. The error is small, and the starting and ending time of the voltage jump is accurately detected. At the same time, by reading the instantaneous amplitude data matrix, the detected voltage amplitude after the temporary rise rises to 435.58, and the error with the theoretical amplitude is 0.02%.

The improved EWT-based disturbance detection model enables rapid identification of voltage anomalies, significantly reducing latency and increasing prediction accuracy. This enhancement directly supports high-frequency data-driven grid decision-making and ensures the robustness of the proposed electric spring compensation framework in complex, nonlinear scenarios.

5 Conclusions

It is imperative to effectively control the power quality in renewable energy power plants, and accurate and real-time power quality disturbance detection is an important premise to control it. In solving the power quality problem, according to electric spring reactive power compensation and EWT, this paper innovatively puts forward the power quality detection and control of renewable energy. This paper presents an electric spring decoupling control method, which can make the critical load voltage stable in given value, and can effectively control and measure the power quality. Specific conclusions are as follows:

1. The electric spring transfers the harmonics and reactive power to the non-critical load through compensation to ensure the safe and stable operation of the critical load, while reducing the loss and improving the power supply efficiency and stability of the grid. Simulation and experimental results verify the correctness of the theoretical analysis. The electric spring has similar harmonic and reactive power compensation functions as active power filter, and can also achieve voltage stability of renewable energy grid connection. As a new type of distributed power electronic equipment, electric spring is different from the centralised compensation of active power filter, and provides a new research idea for harmonic compensation devices.
2. After the voltage sag signal is decomposed by EMD, the IMF1 component retains the characteristics of the signal sag well. The wavelet analysis shows that the instantaneous frequency of the voltage dip signal changes at 0.399 s and 0.651 s, and the actual error is 0.25% and 0.15%, respectively. The error is small, and the starting and ending time of the voltage dip is accurately detected. Meanwhile, through the analysis of the instantaneous amplitude data matrix, the detected voltage amplitude drops to 62.55 V, and the error with the theoretical amplitude is 0.53%.

In future research, the proposed electric spring control strategy can be extended to multi-phase and hybrid AC/DC microgrids to enhance its adaptability in complex distributed power systems. Further studies could also explore the integration of AI-based prediction models for real-time control optimisation, offering more intelligent and adaptive solutions for power quality management in smart grids.

Declarations

Funding: 'Adaptability Study of Flexible Multi-station Automatic Drilling and Tapping Equipment', Anhui Provincial Natural Science Research Project (2022AH052762).

Conflicts of interest: The authors declared that they have no conflicts of interest regarding this work.

References

Abou Hashem, R., Soliman, Y., Al-Sharm, S. et al. (2018) 'Design of an electric spring for power quality improvement in PV-based DC grid', *2018 IEEE Symposium on Computer Applications & Industrial Electronics (ISCAIE)*, IEEE, pp.156–161.

Anu, A.G., Kumar, R.H. and Ushakumari, S. (2020) 'Power quality enhancement of DC micro-grid using DC electric spring', *Advances in Smart Grid Technology: Select Proceedings of PECCON 2019 – Volume I*, Springer Singapore, pp.137–148.

Bebortta, S., Singh, S.K., Rath, M. et al. (2024) 'Dynamic framework towards sustainable and energy-efficient routing in delay tolerant IoT-based WSNs', *International Journal of Systems, Control and Communications*, Vol. 15, No. 1, pp.79–94.

Chen, S., Li, Z., Pan, G. et al. (2022) 'Power quality disturbance recognition using empirical wavelet transform and feature selection', *Electronics*, Vol. 11, No. 2, p.174.

Chiam, D.H., Lim, K.H. and Law, K.H. (2023) 'Global attention-based LSTM for noisy power quality disturbance classification', *International Journal of Systems, Control and Communications*, Vol. 14, No. 1, pp.22–39.

Errami, Y., Obbadi, A. and Sahnoun, S. (2020) 'Control of PMSG wind electrical system in network context and during the MPP tracking process', *International Journal of Systems, Control and Communications*, Vol. 11, No. 2, pp.200–225.

Fu, L., Yan, K. and Zhu, T. (2021) 'PowerCog: a practical method for recognizing power quality disturbances accurately in a noisy environment', *IEEE Transactions on Industrial Informatics*, Vol. 18, No. 5, pp.3105–3113.

Gupta, V., Saxena, N.K., Kanungo, A. et al. (2022) 'PCA as an effective tool for the detection of R-peaks in an ECG signal processing', *International Journal of System Assurance Engineering and Management*, Vol. 13, No. 5, pp.2391–2403.

Lee, C.K., Liu, H., Tan, S.C. et al. (2020) 'Electric spring and smart load: technology, system-level impact, and opportunities', *IEEE Journal of Emerging and Selected Topics in Power Electronics*, Vol. 9, No. 6, pp.6524–6544.

Liang, L., Yi, H., Hou, Y. et al. (2020) 'An optimal placement model for electric springs in distribution networks', *IEEE Transactions on Smart Grid*, Vol. 12, No. 1, pp.491–501.

Mok, K.T., Wang, M.H., Tan, S.C. et al. (2016) 'DC electric springs – a technology for stabilizing DC power distribution systems', *IEEE Transactions on Power Electronics*, Vol. 32, No. 2, pp.1088–1105.

Nagalakshmi, P., Kumar, R.A. and Krishna, K.H. (2022) 'Power quality enhancement in DC microgrids by model predictive control of electric springs', *2022 IEEE 2nd International Conference on Sustainable Energy and Future Electric Transportation (SeFeT)*, IEEE, pp.1–6.

Savrun, M.M. (2021) 'Z-source converter integrated dc electric spring for power quality improvement in dc microgrid', *Engineering Science and Technology, an International Journal*, Vol. 24, No. 6, pp.1408–1414.

Shuo, Y., Tan, S.C., Lee, C.K. et al. (2014) 'Electric spring for power quality improvement', *2014 IEEE Applied Power Electronics Conference and Exposition – APEC 2014*, IEEE, pp.2140–2147.

Solanke, S.S., Jadoun, V.K., Jayalakshmi, N.S. et al. (2022) 'A recapitulation of electric spring for demand side management & power quality mitigation', *IOP Conference Series: Materials Science and Engineering*, IOP Publishing, Vol. 1228, No. 1, p.012028.

Tapia-Tinoco, G., Garcia-Perez, A., Granados-Lieberman, D. et al. (2020) 'Hardware structures, control strategies, and applications of electric springs: a state-of-the-art review', *IET Generation, Transmission & Distribution*, Vol. 14, No. 23, pp.5349–5363.

Wang, M., He, Y., Xu, X. et al. (2021) 'A review of AC and DC electric springs', *IEEE Access*, Vol. 9, No. 18, pp.14398–14408.

Wang, M.H., Mok, K.T., Tan, S.C. et al. (2016) 'Multifunctional DC electric springs for improving voltage quality of DC grids', *IEEE Transactions on Smart Grid*, Vol. 9, No. 3, pp.2248–2258.

Wang, Q., Zha, D., Cheng, M. et al. (2020a) 'Energy management system for DC electric spring with parallel topology', *IEEE Transactions on Industry Applications*, Vol. 56, No. 5, pp.5385–5395.

Wang, Q., Zuo, W., Cheng, M. et al. (2020b) 'Decoupled power control with in-depth analysis of single-phase electric springs', *IEEE Access*, Vol. 8, No. 7, pp.21866–21874.

Xiang, D., Wang, G., Ma, W. et al. (2005) 'Non-integer Harmonic detection method based on FFT and neural network', *Proceedings of the CSEE*, Vol. 25, No. 9, pp.35–39.

Yang, Y., Ho, S.S., Tan, S.C. et al. (2016) 'Small-signal model and stability of electric springs in power grids', *IEEE Transactions on Smart Grid*, Vol. 9, No. 2, pp.857–865.

Yang, Y., Qin, Y., Tan, S.C. et al. (2020) 'Reducing distribution power loss of islanded AC microgrids using distributed electric springs with predictive control', *IEEE Transactions on Industrial Electronics*, Vol. 67, No. 10, pp.9001–9011.

Yu, Z. and Zhang, B. (2025) 'The art of noise modeling and mitigation on power line communication in distributed energy system', *IEEE Transactions on Instrumentation and Measurement*, Vol. 14, No. 9, pp.27–31.

Zhang, X. and Zheng, Z. (2020) 'Application of repetitive control in electric spring', *IEEE Access*, Vol. 8, No. 24, pp.216607–216616.

Zou, Y., Hu, Y. and Cao, S. (2019) 'Model predictive control of electric spring for voltage regulation and harmonics suppression', *Mathematical Problems in Engineering*, Vol. 2019, No. 14, pp.17–28.